

Induced quantum dot probe for material characterization

Yun-Pil Shim,^{1,2} Rusko Ruskov,^{1,2} Hilary M. Hurst,¹ and Charles Tahan¹

¹⁾*Laboratory for Physical Sciences, College Park, Maryland 20740, USA*

²⁾*Department of Physics, University of Maryland, College Park, Maryland 20742, USA*

(Dated: 15 December 2024)

We propose a non-destructive means of characterizing a semiconductor wafer via measuring parameters of an induced quantum dot on the material system of interest with a separate probe chip that can also house the measurement circuitry. We show that a single wire can create the dot, determine if an electron is present, and be used to measure critical device parameters. Adding more wires enables more complicated (potentially multi-dot) systems and measurements. As one application for this concept we consider silicon metal-oxide-semiconductor (MOS) and silicon/silicon-germanium quantum dot qubits relevant to quantum computing and show how to measure low-lying excited states (so-called “valley” states) in a novel way. This approach provides an alternative method for characterization of parameters that are critical for various semiconductor-based quantum dot devices without fabricating such devices.

Semiconductor heterostructures often serve as the substrate for many solid-state devices. For quantum devices such as qubits, their quality depends crucially on the properties of these wafers. Often, these qubit characterization parameters can only be ascertained by fabricating the device and measuring it at cryogenic temperatures. Quantum dots (QDs) in silicon for quantum computing (QC)¹ are a great example. The indirect band-gap of silicon creates low-lying excited (valley) states in the QD heterostructure; if the “valley splitting” is too small, initialization, readout and even gate operation of the qubits is impeded. Optimizing the valley splitting of silicon QD qubits—in addition to other important parameters such as coherence time, charge noise, etc.—is needed for the eventual construction of quantum computers, and is limited by the design-fabrication-test cycle time.

We propose a method of characterizing material properties using a separate probe chip that both creates the dot(s) and measures them. This concept was inspired by the ion trap stylus approach^{2,3} where an ion qubit is trapped on a stylus-like tip that can be brought close to a material to characterize its properties, and also by the scanning nitrogen-vacancy (NV) center tip which can be used to detect magnetic fields at nanoscale for imaging or couple to spin qubits^{4–9}. While these ideas involve putting a qubit on the scanning tip itself, our scheme uses a separate *gate chip* to *induce* a qubit in the material structure under study, then measure those material and qubit parameters of interest using the circuits on the gate chip. Indeed, scanning tunneling microscope (STM) tips have already been used to create effective dots on the surface of InAs^{10,11} and, more recently, Si¹², using tunneling to do spectroscopy. Nondestructive characterization of embedded donor atoms in a semiconductor has also been demonstrated using a scanning tip architecture^{13,14}. Here, we induce the dot qubit within the material in an environment realistic to quantum computing and consider dispersive readout for characterizing material and qubit properties.

To justify the viability of our approach we consider specifically silicon metal-oxide-semiconductor (MOS)

type and silicon/silicon-germanium quantum well (QW) type structures as examples to investigate relevant properties for silicon-based qubit devices. We describe the general geometry of the heterostructure wafer and the gate chip and provide electrostatic simulations of the induced QD. Then, we show how to load the QD and detect the electron by dispersive readout using the quantum capacitance of the induced QD all with the same wire. Finally, methods for measuring the valley splitting based on a much stronger quantum capacitance of the qubit levels at spin-valley anticrossing are discussed using one or more wires.

Figure 1 shows the schematic pictures of a possible setup. The gate chip containing required trapping and measurement circuitry is placed perpendicular above a semiconductor structure, such as MOS [Fig. 1 (a)] or Si/SiGe QW structure [Fig. 1 (b)]. Applying positive voltage V_g to the gate wire induces a confining electrostatic potential in the 2D quantum well in the structure [Fig. 1 (c)] and orbital wavefunctions show typical 2D QD orbital characters [Fig. 1 (d)]. Electrons can be trapped into the induced QD as was depicted by red regions in Fig. 1 (a) for MOS and (b) for QW. The energy levels of the induced QDs have nonzero second derivative w.r.t. the applied voltage (i.e. a quantum capacitance), allowing for a dispersive readout by coupling to a detector circuit which can be integrated in the gate chip^{15–18}.

We performed electrostatic simulation of the device¹⁹ using dimensions for MOS and QW devices that are typically used in experiments. For a MOS structure^{20–23}, a silicon oxide layer of 10nm overlays the silicon substrate of $\gg 200$ nm. For a QW structure^{24,25}, a strained silicon quantum well of 10nm is sandwiched between a $\gg 200$ nm SiGe substrate and a 40nm SiGe spacer which is capped by 10nm of silicon. We choose a reasonable and manufacturable gate chip design to demonstrate the main concepts in this work. The gate wire size is chosen to be 10nm \times 10nm and 1 μ m long, and 10nm away from the top of the heterostructure. We considered different sizes of gate wafers as well as a bare metallic wire tip with no gate wafer for the simulations and obtained qualitatively

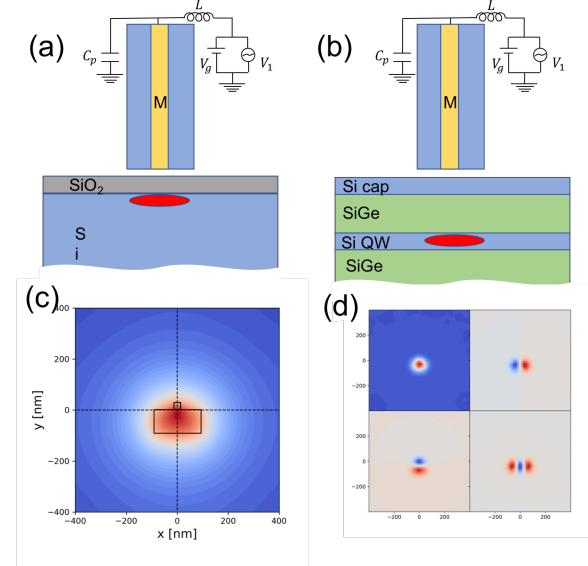


FIG. 1. Schematic diagram of the device, for MOS (a) and QW (b) structures. A chip with a metallic wire or gate denoted by M (and other necessary circuitry; L is the inductance and C_p is unavoidable parasitic capacitance) on it is positioned above the semiconductor heterostructure to induce a QD for easy, non-invasive characterization. DC and AC voltages can be simultaneously applied to the gate wire for inducing the quantum dot and its characterization. QD confining potential and four lowest orbitals in MOS device with a DC gate voltage $V_g=0.02\text{V}$ are shown in (c) and (d), respectively. Si/SiGe QW device has slightly larger QD than the MOS device for a given V_g in our simulation. The position of the induced QD is slightly off the gate wire position due to the presence of the silicon wafer on which the gate wire is placed.

similar results. To be specific, we present below results for the gate wire on a silicon wafer of 100nm depth and 200nm width.

To conduct measurements of useful device properties, especially for properties relevant for spin qubits, we need to populate the induced quantum dot with a controlled number of electrons. This can be achieved in a number of different ways: e.g., (i) an electron-hole pair can be generated near the induced QD by light, and the electron is trapped to the QD while the hole is pushed away from the QD by the electrostatic force, or (ii) one can dope the semiconductor by implanting donors in a specific region (or use large “electron bath” gate^{15,17}) and use the dot accumulation wire to load electrons from the doped region into the QD (one could then possibly move the electron to another area on the chip as in the STM induced QD device¹²). Once isolated, the dot gate voltage can be tuned to enhance the quantum capacitance while maintaining single occupation.

We can detect the charge in the QD via dispersive readout^{15–18} by incorporating a tank-circuit (often superconducting) resonator (typically with frequency ω_r of a few hundred MHz to a few GHz) into the gate wire and

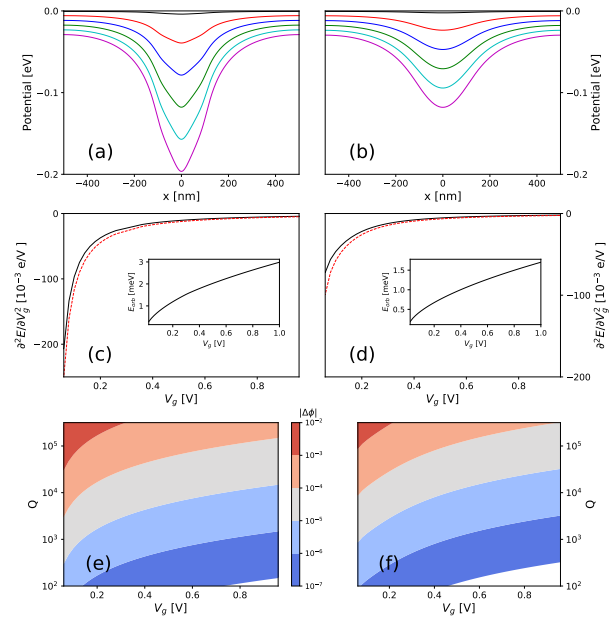


FIG. 2. Simulation of the QD potential and the quantum capacitance of the induced QD. (a) QD potential on MOS device, for various gate voltages $V_g=0.02, 0.2, 0.4, 0.6, 0.8, 1.0\text{V}$ from top to bottom. (b) is the QD potential for Si/SiGe device, for the same V_g values. (c) and (d) are the second derivative of the two lowest energy levels of the induced QD for MOS and QW structures, respectively. The solid black curves are for the ground orbitals, and dashed red curves are for the first excited orbitals. $\partial^2 E_i / \partial V_g^2$ is in unit of 10^{-3}eV/V which is $1.6 \times 10^{-4}\text{ aF}$. Insets show the orbital energy splitting between two lowest orbitals vs the applied voltage V_g . (e) and (f) show the calculated phase shift of the reflected signal as a function of the applied voltage V_g and the quality factor Q of the resonator circuit for MOS and QW devices, respectively, assuming the induced dot is singly occupied.

accumulated QD [e.g., Fig. 1(a)], and then sending and reflecting resonant microwaves to it. There would be no phase shift of the reflected signal from an empty dot, but if there is a trapped electron, the reflected signal will be phase shifted if the quantum capacitance^{26–32} of the electron energy level is large enough. We send an rf-signal (along with the DC voltage V_g): $V = V_g + V_1 \cos(\omega_r t)$. In addition to the conventional capacitance of the gate-to-heterostructure QD, C_{MOS} , and a distributed parasitic capacitance C_p of the gate to the ground plane, as was depicted in Fig.1 (a) and (b), there will be a quantum capacitance $C_{q,i} = \alpha_c^2 \frac{\partial^2 E_i}{\partial V_g^2}$ of the induced QD, including the lever arm $\alpha_c \equiv \frac{C_c}{C_c + C_d}$ of the tip-to-dot capacitive coupling (here C_c and C_d are the tip-to-dot and dot-to-ground capacitances, respectively; for further estimations we assume $\alpha_c \sim 1$). The quantum capacitance arises from the non-linear voltage response of the QD’s energy levels³², $E_i(V_g) = E_i(V_g^0) + \frac{\partial E_i}{\partial V_g} \delta V_g + \frac{1}{2} \frac{\partial^2 E_i}{\partial V_g^2} \delta V_g^2$, assuming slow in time voltage perturbation δV_g . It leads

to a frequency shift of the tank-circuit³², and the corresponding phase shift of the reflected signal due to C_q would be^{15,16}

$$\Delta\phi \simeq Q \frac{\delta C}{C_{\text{tot}}} \equiv Q \frac{C_q}{C_p + C_{\text{MOS}} + C_q}, \quad (1)$$

where the Q-factor is defined via the tank-circuit relaxation $\kappa = \omega_r/Q$. [For a single QD level the non-linear voltage response arises from the spatial change of the orbitals, which is often neglected in Hubbard-like Hamiltonians. We recently showed the differences between a Hubbard-like Hamiltonian and the actual induced QD system and its consequences on QD devices.³³] Figure 2 (a) and (b) show the QD confining potentials at various V_g values for MOS and QW devices, respectively. The second derivative of the orbital energy levels w.r.t the applied V_g is shown in Fig. 2 (c) for MOS and (d) for QW. The absolute value of the quantum capacitance is larger for smaller gate voltage V_g and can be as large as $\lesssim 0.03$ aF for MOS and $\lesssim 0.01$ aF for QW at $V_g = 0.02$ V, for the geometry studied in this work.

For typical low Q tank-circuits^{15,17} having C_{tot} of a few hundred fF (and a frequency in the few hundred MHz range) a capacitance change at level of a few aF is measurable¹⁷, leading to a phase shift $\Delta\phi \approx 10^{-4} - 10^{-5}$. Figure 2 (e) and (f) show the calculated phase shift for $C_{\text{tot}} = 1000$ fF, vs. Q and V_g from Eq. (1) (assuming $\frac{\delta C}{C_{\text{tot}}} \ll 1/Q$). The sensitivity to measure a small quantum capacitance will increase for moderately large tank-circuit Q-factors, (e.g., the recently proposed high-kinetic inductance nano-wire resonators³⁴ with frequency of a few GHz and $Q \approx 10^3$ can be used in our proposed vertical gate circuit). As an example, for $C_q \gtrsim 0.01$ aF as per the simulation, and a reachable resonator parameters³⁴: $C_{\text{tot}} \approx 30$ fF $Q \approx 10^3$, one can obtain $\Delta\phi \gtrsim 3 \times 10^{-4}$, which is readily measurable^{16,17}. The lowest detectable C_q may be limited by unwanted variation in gate-to-QD capacitance as a function of gate voltage (e.g., due to interface traps below the QD gate¹⁷).

If the device is in a configuration where the induced QD is close to an electron reservoir or another quantum dot, then the charge stability diagram can be mapped out directly using the tunneling capacitance,²⁹ where the response signal peaks at a charge transition (similar to Ref. [15]).

As an example of critical material parameters that the separate gate chip could measure, we now discuss how to measure the valley splitting in a silicon wafer. We first examine the case of a single QD with one electron. Following the ideas of Ref. [20], a relatively small accumulation mode QD as in Ref. [17] can ensure that the orbital splitting is much larger than the valley splitting, $E_{\text{orb}} \gg E_{\text{VS}}$, which allows us to consider only the lowest orbital states in the following analysis. Experimentally, $E_{\text{VS}} = 300 - 800$ μeV and $E_{\text{orb}} = 2 - 8$ meV in small QDs in a MOS device²⁰ and also $E_{\text{VS}} = 80 - 100$ μeV and $E_{\text{orb}} = 0.5$ meV in another MOS device³⁵. For Si/SiGe quantum dots, E_{VS} could be of the order of 80 – 100 μeV ,

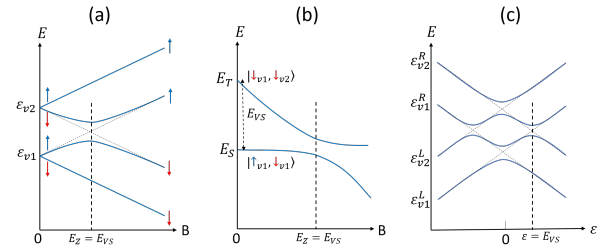


FIG. 3. Schematic energy level diagrams for valley-splitting measurement. (a) A QD with a single electron in an external magnetic field. The spin states of each valley states split due to the Zeeman splitting, and when the Zeeman splitting E_Z is equal to the valley splitting E_{VS} , there is an anti-crossing of energy levels between the second and third levels. The energy curvature w.r.t. gate voltage V_g is maximal at the anticrossing, Eq. (2), since $\frac{\partial^2 E_i}{\partial V_g^2} \propto \frac{\partial^2 E_i}{\partial B^2}$ for the regime considered. (b) A QD with two electrons in it has singlet and triplet states, which anti-cross at $E_Z = E_{\text{VS}}$. (c) A DQD with a single electron with tunable detuning of the dot energy levels. When the detuning reaches $\varepsilon = E_{\text{VS}}$ these anti-crossings affect the quantum capacitance and can be measured by rf-reflectometry.

or it could be much smaller. In the simulation of induced dots the above is satisfied as E_{orb} is of the order of meV [see insets of Fig. 2 (c) and (d)].

The valley splitting, $E_{\text{VS}} \propto aV_g$, depends linearly on the applied top gate voltage²⁰. By applying an in-plane magnetic field, the lowest two valley states are Zeeman split (with energy splitting E_Z) into 4 levels, as is shown in Fig. 3(a). The levels 2 and 3 (with different valley content) anti-cross when $E_Z = E_{\text{VS}}$, which leads to levels' energy curvature w.r.t. the gate voltage V_g . Indeed, the splitting at anti-crossing, $\Delta_a \propto |\mathbf{r}_{v1,v2}| E_{\text{VS}} (\beta_D - \alpha_R)$ can be phenomenologically parameterized with an (intervalley) dipole matrix element $\mathbf{r}_{v1,v2}$ ^{20,36}, implying a charge re-distribution as a result of interface-induced intervalley tunneling and spin-orbit couplings³⁷. We have estimated²⁰ $\Delta_a = 10^{-4} - 10^{-3} E_{\text{VS}}$, using a Rashba/Dresselhaus spin-orbit interactions, α_R, β_D , induced at the heterostructure interface³⁷. The levels 2 and 3 then read: $E_{2,3}(V_g) = \frac{1}{2}[E_{\text{VS}}(V_g) \mp \sqrt{(E_{\text{VS}}(V_g) - E_Z(B))^2 + \Delta_a(V_g)^2}]$. This was used to describe the relaxation “hot spot” observed in the experiment, which is mainly due to acoustic phonon emission²⁰.

Given this explicit level structure we calculate the curvature of the levels with respect to the gate voltage V_g , obtaining the levels' quantum capacitances, $C_{q,i}$ (this quantifies the non-linear response of the QD system³²). In the magnetic field at anti-crossing [Fig. 3 (a)], these quantum capacitances may be strongly enhanced w.r.t. that of the simple orbitals discussed above. The ground state has zero curvature ($C_{q,1}=0$) from this effect, while for levels 2 and 3 one gets $C_{q,2} = -C_{q,3}$, and

$$C_{q,3} \simeq \frac{a^2}{2\Delta_a} / \left[\left(\frac{E_{\text{VS}} - E_Z}{\Delta_a} \right)^2 + 1 \right]^{3/2}, \quad (2)$$

with the capacitances sharply peaked near the anti-crossing (using a simple model with linear dependence on V_g for the valley splitting³⁷). With the experimentally estimated Δ_a and valley splitting slope²⁰ $a_{\text{exp}} \simeq 0.64 \text{ meV/V}$, we obtain (for $E_{\text{VS}} = 100 \mu\text{eV}$)

$$|C_{q,2,3}| \simeq 0.3 - 3 \text{ aF}, \quad (3)$$

which should be measurable in experiments^{16,17}. Another capacitance contribution may appear due to fast relaxation processes³¹. While the relaxation rate Γ_{rel} strongly increases at the spin-valley anti-crossing for a single electron QD²⁰ (reaching $10^7 - 10^8 \text{ s}^{-1}$), it is much slower than the chosen tank-circuit frequencies, $\Gamma_{\text{rel}} \ll \omega_r$, thus suppressing this capacitance contribution³¹. A way to enhance $|C_{q,2,3}|$ is to use the in-plane magnetic field with an angle such that Δ_a becomes much smaller³⁷, however making Δ_a smaller will narrow the region where C_q is significantly non-zero.

By scanning (sweeping) the magnetic field we will register a sharp peak of phase change of the reflected signal when the Zeeman splitting is $E_Z = E_{\text{VS}}$. For this to work, we need to populate the excited states by choosing a temperature comparable to the valley splitting, e.g. for $E_{\text{VS}} = 100 \mu\text{eV}$ the temperature should be $T \sim 1 \text{ K}$. Since $E_{\text{VS}} \gg \Delta_a$, the populations of the levels 2 and 3 in Fig. 3(a) will be comparable, thus leading to an effective quantum capacitance suppression by $\Delta_a/kT \sim \Delta_a/E_{\text{VS}} \sim 10^{-3}$.

A way to mitigate these effects would be to use a single QD with two electrons. As shown in Fig. 3(b), the lowest two levels now anti-cross at $E_Z = E_{\text{VS}}$ with an anti-crossing splitting $\Delta_a^{2e} \approx \Delta_a$ (scf. Ref. [20]), and the quantum capacitance is the same as in the 1-electron case, Eqs. (2) and (3), while the relaxation is strongly suppressed at anti-crossing. Also, the suppression effect due to temperature will not be as strong as in the 1-electron case, since $kT \sim \omega_r \lesssim 1 \text{ GHz}$ and so $\Delta_a/kT \sim \Delta_a/\omega_r \sim 10^{-1} - 10^{-2}$. Since, however, we are in a regime $\omega_r \gg \Delta_a$ (opposite to that where a quantum capacitance approximation is valid) the effective quantum capacitance is suppressed by a form factor: $C_{q,\text{eff}} \simeq C_q \left(\frac{\Delta_a}{\omega_r} \right)^2$. E.g., for $E_{\text{VS}} \lesssim 100 \mu\text{eV}$ the suppression factor is $\left(\frac{\Delta_a}{\omega_r} \right)^2 \approx 1/40^2$. Thus, this method would be sufficient to measure not too small valley splitting.

An alternative method to measure the valley splitting with a slightly more complicated gate circuit is to induce a double QD using two or three gate wires on the gate chip. Let us consider a DQD with a single electron, assuming each QD has the same valley splitting. The detuning between the QDs can be changed by tuning the voltages on the two QD-defining gates. At zero detuning ($\varepsilon = 0$), one is at the degeneracy point of the lower eigenvalue $v1$ -electrons. [$v1$ is the lower valley and $v2$ is the upper valley states. See Fig. 3(c)]. The left-right tunneling t between the dots defines the

splitting at anti-crossing, $2t$. One then can measure the change of the reflected signal at the degeneracy point (where the energy curvature is maximal) using a tank-circuit frequency $\omega_r \ll 2t$. By sweeping the detuning to $\varepsilon = E_{\text{VS}}$ the $v1$ -electron from the left can tunnel to the $v2$ -level from the right. This tunneling possibility forms another anti-crossing and corresponding splitting (assume the same $2t$). (This kind of tunneling is briefly discussed in Ref. [35] and then at length in Ref. [38].)

To measure the valley splitting, one starts at $\varepsilon = 0$, and populates the lowest two levels by temperature. One then moves (faster than the relaxation time T_1) to a detuning $\varepsilon = E_{\text{VS}}$, while sending a microwave with $\omega_r \ll 2t$, to encounter a sharp change in the reflected phase (provided that $t \ll E_{\text{VS}}$). This can be fulfilled for $2t \approx 2 - 4 \text{ GHz}$ and $\omega_r \approx 0.5 - 1 \text{ GHz}$. Once $\varepsilon = E_{\text{VS}}$ is reached, the reflected signal changes accordingly, due to maximal quantum capacitance $C_q = \frac{e^2}{2t}$ similar to the experiment of Pettersson et al.²⁹. The quantum capacitance at this anti-crossing is estimated of the order of 10 fF , which is several orders of magnitude larger than at the spin-valley anti-crossing discussed above. In order to be able to distinguish the anti-crossings at $\varepsilon = 0$ and at $\varepsilon = E_{\text{VS}}$, one needs $E_{\text{VS}} \gtrsim 2t$ which sets the lowest measurable valley splitting, $E_{\text{VS}} \gtrsim 5 - 10 \mu\text{eV}$. The main difference of this proposal from that of Ref. [38] is that the probing signal is far off resonance with the level splitting, at a constant tank-circuit frequency $\omega_r \ll 2t$, and the signature of valley splitting is easier to measure. These last two cases - doubly occupied single QD and a singly occupied DQD - may be the easiest to experimentally implement as a first verification of this proposed methodology.

Finally, we note that an additional (tunable) microwave field can be introduced to the above proposed experiments to drive transitions between quantum dot states, which may allow for further or improved characterization (and also introduces another absolute energy scale to compare to, in addition to the magnetic field).

The proposal presented in this paper requires sensitive measurement of small (quantum) capacitance changes, C_q , in sub-aF to aF range. The signal due to C_q may be obscured, however, in the presence of noise of the large fluctuating capacitances, C_{MOS} , C_p (see Fig. 1). For example, fluctuations via the voltage dependence of $C_{\text{MOS}}(V_g)$ are attributed to the charging of interface traps below the QD gate¹⁷; the corresponding noise variation would be $\Delta C_{\text{MOS}}^{\text{noise}} = \left| \frac{\partial C_{\text{MOS}}}{\partial V_g} \right| \sqrt{\frac{S_V}{2t_{\text{av}}}}$ where S_V is the voltage spectral density and t_{av} is an averaging time. It was experimentally shown that below a sample-specific voltage threshold, $V_g < V_{\text{th}}$, the capacitance derivative is small and a capacitance change of $\approx 1.5 \text{ aF}$ was resolved¹⁷. Another type of noise may enter through mechanical fluctuations of the tip. See e.g. experiments with Scanning Microwave Microscopy (SMM)^{14,39}. In an experiment of near-field SMM³⁹ the (slow) resonator frequency fluctuations are tracked and stabilized via a feedback loop allowing longer averaging time to reduce the

noise; a sensitivity of $(0.06 \text{ aF})^2/\text{Hz}$ was limited by mechanical noise³⁹. Since in our proposed experiment the tip is not moving, the mechanical noise may be reduced, eventually allowing for valley splitting measurement via a tip-induced QD in the Si heterostructure.

Inducing quantum dots instead of fabricating them offers the potential for non-destructive characterization either locally or across a wafer, speeding optimization of materials and quantum devices such as qubits. Our concept is applicable to other materials and systems as the inducing and measurement chip can be fabricated on a substrate different from the materials system under consideration. We show that inducing QDs and measuring valley splitting in silicon devices is plausible with current experimental technology. Induced QD devices and the actual quantum devices built on the wafer will be different, but they share many critical aspects of the underlying material. Characterization of the induced QD devices will provide useful information of the yet-to-be-built devices. Based on this concept, other materials and systems (germanium, holes instead of electrons, topological systems, etc.) and qubit approaches (encoded qubits, different readout techniques, even linear arrays of qubits making small quantum computers) can be explored without actually fabricating the quantum dots themselves.

We thank Bob Butera and Michael Dreyer for helpful discussion. H.M.H. acknowledges support from the NPSC fellowship.

- ¹F. A. Zwanenburg, A. S. Dzurak, A. Morello, M. Y. Simmons, L. C. L. Hollenberg, G. Klimeck, S. Rogge, S. N. Coppersmith, and M. A. Eriksson, *Rev. Mod. Phys.* **85**, 961 (2013).
- ²R. Maiwald, D. Leibfried, J. Britton, J. C. Bergquist, G. Leuchs, and D. J. Wineland, *Nat. Phys.* **5**, 551 (2009).
- ³C. L. Arrington, K. S. McKay, E. D. Baca, J. J. Coleman, Y. Colombe, P. Finnegan, D. A. Hite, A. E. Hollowell, R. Jördens, J. D. Jost, D. Leibfried, A. M. Rowen, U. Warring, M. Weides, A. C. Wilson, D. J. Wineland, and D. P. Pappas, *Rev. Sci. Instrum.* **84**, 085001 (2013).
- ⁴J. M. Taylor, P. Cappellaro, L. Childress, L. Jiang, D. Budker, P. R. Hemmer, A. Yacoby, R. Walsworth, and M. D. Lukin, *Nat. Phys.* **4**, 810 (2008).
- ⁵C. L. Degen, *Appl. Phys. Lett.* **92**, 243111 (2008).
- ⁶J. R. Maze, P. L. Stanwix, J. S. Hodges, S. Hong, J. M. Taylor, P. Cappellaro, L. Jiang, M. V. G. Dutt, E. Togan, A. S. Zibrov, A. Yacoby, R. L. Walsworth, and M. D. Lukin, *Nature* **455**, 644 (2008).
- ⁷G. Balasubramanian, I. Y. Chan, R. Kolesov, M. Al-Hmoud, J. Tisler, C. Shin, C. Kim, A. Wojcik, P. R. Hemmer, A. Krueger, T. Hanke, A. Leitenstorfer, R. Bratschitsch, F. Jelezko, and J. Wrachtrup, *Nature* **455**, 648 (2008).
- ⁸P. Maletinsky, S. Hong, M. S. Grinolds, B. Hausmann, M. D. Lukin, R. L. Walsworth, M. Loncar, and A. Yacoby, *Nat. Nanotechnol.* **7**, 320 (2012).
- ⁹F. Casola, T. van der Sar, and A. Yacoby, *Nat. Rev. Mater.* **3**, 17088 (2018).
- ¹⁰C. Wittneven, R. Dombrowski, M. Morgenstern, and R. Wiesendanger, *Phys. Rev. Lett.* **81**, 5616 (1998).
- ¹¹R. Dombrowski, C. Steinebach, C. Wittneven, M. Morgenstern, and R. Wiesendanger, *Phys. Rev. B* **59**, 8043 (1999).
- ¹²J. Salfi, B. Voisin, A. Tankasala, J. Bocquel, M. Usman, M. Y. Simmons, L. C. L. Hollenberg, R. Rahman, and S. Rogge, *Phys. Rev. X* **8**, 031049 (2018).
- ¹³E. Bussmann, M. Rudolph, G. S. Subramania, S. Misra, S. M. Carr, E. Langlois, J. Dominguez, T. Pluym, M. P. Lilly, and M. S. Carroll, *Nanotechnology* **26**, 085701 (2015).
- ¹⁴G. Gramse, A. Kölker, T. Lim, T. J. Z. Stock, H. Solanki, S. R. Schofield, E. Brinciotti, G. Aeppli, F. Kienberger, and N. J. Curson, *Sci. Adv.* **3**, e1602586 (2017).
- ¹⁵J. I. Colless, A. C. Mahoney, J. M. Hornibrook, A. C. Doherty, H. Lu, A. C. Gossard, and D. J. Reilly, *Phys. Rev. Lett.* **110**, 046805 (2013).
- ¹⁶M. Gonzalez-Zalba, S. Barraud, A. Ferguson, and A. Betz, *Nat. Commun.* **6**, 6084 (2015).
- ¹⁷A. Rossi, R. Zhao, A. S. Dzurak, and M. F. Gonzalez-Zalba, *Appl. Phys. Lett.* **110**, 212101 (2017).
- ¹⁸M. Urdampilleta, D. J. Niegemann, E. Chanrion, B. Jadot, C. Spence, P.-A. Mortemousque, C. Bäuerle, L. Hutin, B. Bertrand, S. Barraud, R. Maurand, M. Sanquer, X. Jehl, S. D. Franceschi, M. Vinet, and T. Meunier, “Gate-based high fidelity spin readout in a CMOS device,” (2018), arXiv:1809.04584 [cond-mat].
- ¹⁹COMSOL Multiphysics® v.5.3. www.comsol.com. COMSOL AB, Stockholm, Sweden.
- ²⁰C. H. Yang, A. Rossi, R. Ruskov, N. S. Lai, F. A. Mohiyaddin, S. Lee, C. Tahan, G. Klimeck, A. Morello, and A. S. Dzurak, *Nat. Commun.* **4**, 2069 (2013).
- ²¹M. Veldhorst, J. C. C. Hwang, C. H. Yang, A. W. Leenstra, B. de Ronde, J. P. Dehollain, J. T. Muñonen, F. E. Hudson, K. M. Itoh, A. Morello, and A. S. Dzurak, *Nat. Nanotechnol.* **9**, 981 (2014).
- ²²R. Maurand, X. Jehl, D. Kotekar-Patil, A. Corra, H. Bohuslavskyi, R. Laviéville, L. Hutin, S. Barraud, M. Vinet, M. Sanquer, and S. D. Franceschi, *Nat. Commun.* **7**, 13575 (2016).
- ²³M. A. Fogarty, K. W. Chan, B. Hensen, W. Huang, T. Tanttu, C. H. Yang, A. Laucht, M. Veldhorst, F. E. Hudson, K. M. Itoh, D. Culcer, T. D. Ladd, A. Morello, and A. S. Dzurak, “Integrated silicon qubit platform with single-spin addressability, exchange control and robust single-shot singlet-triplet readout,” (2017), arXiv:1708.03445 [cond-mat].
- ²⁴E. Kawakami, P. Scarlino, D. R. Ward, F. R. Braakman, D. E. Savage, M. G. Lagally, M. Friesen, S. N. Coppersmith, M. A. Eriksson, and L. M. K. Vandersypen, *Nat. Nanotechnol.* **9**, 666 (2014).
- ²⁵D. M. Zajac, T. M. Hazard, X. Mi, K. Wang, and J. R. Petta, *Appl. Phys. Lett.* **106**, 223507 (2015).
- ²⁶D. V. Averin, A. B. Zorin, and K. K. Likharev, *Sov. Phys. JETP* **61**, 407 (1985).
- ²⁷T. Duty, G. Johansson, K. Bladh, D. Gunnarsson, C. Wilson, and P. Delsing, *Phys. Rev. Lett.* **95**, 206807 (2005).
- ²⁸M. A. Sillanpää, T. Lehtinen, A. Paila, Y. Makhlin, L. Roschier, and P. J. Hakonen, *Phys. Rev. Lett.* **95**, 206806 (2005).
- ²⁹K. D. Petersson, C. G. Smith, D. Anderson, P. Atkinson, G. A. C. Jones, and D. A. Ritchie, *Nano Lett.* **10**, 2789 (2010).
- ³⁰A. Cottet, C. Mora, and T. Kontos, *Phys. Rev. B* **83**, 121311(R) (2011).
- ³¹R. Mizuta, R. M. Otxoa, A. C. Betz, and M. F. Gonzalez-Zalba, *Phys. Rev. B* **95**, 045414 (2017).
- ³²R. Ruskov and C. Tahan, “Quantum-limited measurement of spin qubits via curvature coupling to a cavity,” (2017), arXiv:1704.05876v1 [cond-mat].
- ³³Y.-P. Shim and C. Tahan, *Phys. Rev. B* **97**, 155402 (2018).
- ³⁴N. Samkharadze, G. Zheng, N. Kalhor, D. Brousse, A. Sammak, U. C. Mendes, A. Blais, G. Scappucci, and L. M. K. Vandersypen, *Science* **359**, 1123 (2018).
- ³⁵X. Hao, R. Ruskov, M. Xiao, C. Tahan, and H. Jiang, *Nat. Commun.* **5**, 3860 (2014).
- ³⁶J. K. Gamble, M. A. Eriksson, S. N. Coppersmith, and M. Friesen, *Phys. Rev. B* **88**, 035310 (2013).
- ³⁷R. Ruskov, M. Veldhorst, A. S. Dzurak, and C. Tahan, *Phys. Rev. B* **98**, 245424 (2018).
- ³⁸G. Burkard and J. R. Petta, *Phys. Rev. B* **94**, 195305 (2016).
- ³⁹S. E. de Graaf, A. V. Danilov, A. Adamyan, and S. E. Kubatkin, *Rev. Sci. Instrum.* **84**, 023706 (2013).